Nano Research

Open Access

Research Article

Diffusion-driven light emission in branched GaInP nanowire LEDs enabled by indirect–direct bandgap engineering

Yue Zhao[1], Kristi Adham[1,†], Haonan Chen[1,2], and Magnus T. Borgström[1,2] ✉

[1] *Solid State Physics and NanoLund, Lund University, Box 118, SE-22100 Lund, Sweden*
[2] *Wallenberg Initiative Materials Science for Sustainability, Department of Physics, Lund university, SE-22100 Lund, Sweden*
[†] *Present address: AWA Sweden AB, SE-22100 Lund, Sweden*

Cite this article: *Nano Research*, **2026**, *19*, 94908799. https://doi.org/10.26599/NR.2026.94908799

ABSTRACT: Semiconductor nanowires (NWs) offer unique opportunities for next-generation optoelectronic devices. In this work, we investigate charge carrier diffusion induced branched NW light-emitting diodes (LEDs) with designed bandgap heterojunctions. Emission from epitaxially grown arrays of direct bandgap branch NWs on indirect bandgap GaInP core NWs is characterized. We significantly suppress radiative recombination in the indirect bandgap core while promoting carrier diffusion toward the branches. Temperature-dependent electroluminescence measurements reveal different recombination mechanisms in the indirect bandgap core and direct bandgap branch NWs. Dominant branch emission is achieved by use of indirect bandgap core NWs, which enables the design of monochromatic branched NW LEDs with potentially high light extraction efficiency. These results demonstrate an attractive pathway toward high efficiency NW-based LEDs.

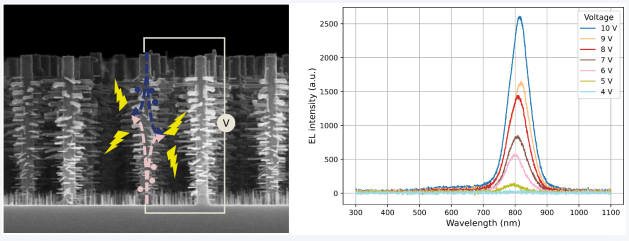

KEYWORDS: nanowires, light-emitting diodes, charge carrier diffusion, indirect bandgap

1 Introduction

Nanowires (NWs) have attracted researchers' interest as nanoscale building blocks for next-generation optoelectronic devices including solar cells [1–3], photodetectors [4, 5], light-emitting diodes (LEDs) [6–8], and lasers [9, 10]. Compared to traditional planar structures, strain release can occur radially in NWs due to their small diameter [11, 12]. Therefore, complex heterostructure synthesis to tune the bandgap for novel applications, without lattice mismatch limitations is feasible [13]. Several studies have been conducted on the formation of axial junctions along NWs with quantum wells embedded by tuning the material compositions [14, 15], as well as radial junctions in core–shell structures [7, 16]. In addition, by enhanced electro-optical properties at nanoscale, much less semiconductor material is typically needed for device structures relying on geometrically enhanced light interaction [17]. For example, the surface coverage of 1 μm pitch hexagonal patterned NWs with a diameter of 130 nm is only 1.53% of the substrate area.

Received: March 20, 2026; **Revised:** April 29, 2026
Accepted: April 30, 2026

✉Address correspondence to magnus.borgstrom@fysik.lu.se

With these advantages, NW LEDs have been widely investigated using different material combinations for light emission in the visible range for applications such as displays [18–20], and with varied geometries in terms of diameters and densities for better light extraction efficiency and emission [21, 22]. We recently reported on a novel type of architecture for LEDs, charge carrier diffusion induced NW LEDs [8, 23] designed like "nanotrees" where lower bandgap branch NWs are grown on the sidewalls of higher bandgap core NWs allowing light emission directly into free space instead of having the active area as multi quantum wells embedded in semiconductor material. The core NWs were axially pin-doped and by applying a forward bias over the core NWs, injected charge carriers diffuse from the core to branch NWs where carrier recombination and light emission occur. Light emission from both the core and the branch NWs were observed, with transition energy corresponding to that of the bandgap of the cores and the branches. Owing to the subwavelength size of the branch NWs, the light extraction efficiency of the branched NW LEDs is expected to be enhanced [17] as compared to traditional planar LEDs that suffer from total internal reflection because of the large difference in refractive index of the light emitting material and that of the air.

In this study, indirect bandgap core NWs were designed and synthesized to enhance the light emission from the branch NWs rather than from the core NWs. This increases the diffusion

induced by the bandgap differences between the core and branch NWs and impedes light emission from the core NWs due to their indirect bandgap nature [24]. We fabricated branched NW LEDs with 83.7% Ga in the indirect bandgap $Ga_xIn_{1-x}P$ core NW array and direct bandgap branch NWs emitting at approximately 810 nm. Light emission was observed from the branch NWs only, until the bias voltage exceeded approximately 12 V at room temperature. We compared the performance of branched NW LEDs made from direct and indirect bandgap cores. We investigated the carrier recombination mechanism by use of temperature-dependent electroluminescence (EL) characterization to further increase our understanding of the "nanotree" structure and its LED performance.

2 Experimental methods

2.1 Branched NW synthesis

Talbot displacement lithography was applied to a 2-inch p-doped (Zn) InP(111) B wafer to produce a hexagonal pattern of holes [25] with a diameter of 200 nm and a pitch of 1000 nm (Eulitha) in the photoresist. A 65 nm thick Au thin layer was evaporated by e-beam evaporator (Temescal) on the wafer, followed by a lift-off step. The wafer was then diced into 9 mm × 11 mm rectangular pieces to be used as substrates for NW-synthesis. The axially pin-doped indirect bandgap core wire array was grown by use of metal-organic vapor phase epitaxy (MOVPE, Aixtron 200/4) at 100 mbar with a total flow of 13 L/min using hydrogen as carrier gas. The substrate was prepared for NW synthesis using a low temperature nucleation at 280 °C for 1 min for pattern fidelity [26] and high temperature annealing at 550 °C for 10 min to desorb surface oxides. Subsequently, the reactor temperature was reduced, and NW synthesis was performed at 440 °C. The molar fractions of each precursor during growth are shown in Tables S1 and S2 in the Electronic Supplementary Material (ESM) for the indirect and direct bandgap core NWs separately. Triethylgallium (TEGa), trimethylindium (TMIn), and phosphine (PH_3) were used as precursors for synthesis [27, 28]. Diethylzinc (DEZn) and hydrogen sulfide (H_2S) were used as precursors for p-type and n-type doping, respectively.

To enable the growth of branch NWs on the sidewall of the core NWs, Au nanoparticles were first deposited on the sidewall of core NWs by use of galvanic displacement [29], immersing the sample into 0.4 mM $HAuCl_4$ solution for 30 s. The sample was then spin-coated with photoresist and exposed to ultraviolet (UV) light to reveal the tip of the core wires [30] and to cover (protect) the Au nanoparticles deposited on the sidewalls. Native oxide etching using H_2SO_4:H_2O (1:400) for 25 s was followed by 25 s of Au etchant (potassium iodide, KI) to etch away the seed Au particles used for the core wire growth to avoid axial growth during subsequent branch synthesis. After cleaning the photoresist, the sample was transferred into the MOVPE for growth of the branches. The branches are nominally intrinsic $Ga_xIn_{1-x}P$, as depicted in Figs. 1(a) and 1(b). The molar fractions of the precursors are listed in Table S3 in the ESM.

2.2 Charge carrier diffusion induced NW LEDs fabrication

The samples were fabricated into LEDs after the core and branch NWs synthesis. We used atomic layer deposition (ALD, Savannah) to deposit a 30 nm silicon oxide (SiO_x) layer to electrically isolate the NWs and prevent short circuiting of the devices. Then the samples were spin-coated with photoresist for the purpose of planarization and exposed by UV light to reveal the NW tips [30]. Reactive ion etching (RIE, Trion) was used to etch back the SiO_x to open the coated NW tips for deposition of electrical contacts. The first photolithography defined the active areas of multiple LEDs, with different sizes of 100 μm × 100 μm (Fig. 1(c)), 200 μm × 200 μm, 400 μm × 400 μm, and 800 μm × 800 μm. There are approximately 11 thousand NWs in the 100 μm × 100 μm device that will be connected in parallel by sputtering (AJA Orion 5) of a 150 nm thick indium tin oxide (ITO) as transparent conducting layer, followed by a second photolithography step to isolate each LED. The final photolithography step defined the metal contact area for each LED. The metal contact was 20 nm Ti and 400 nm Au evaporated via an e-beam evaporator (Temescal). An overnight lift-off step in acetone was used. The final view of a finished device is shown in Fig. 1(c) with a schematic drawing of the cross-sectional view in Fig. 1(d).

2.3 LED characterization

X-ray diffraction (XRD, Bruker D8 Discover) was used to analyse the Ga composition of the core NW arrays after growth. The morphology of the sample surface was investigated using scanning electron microscopy (SEM, Zeiss LEO 1560). Current–voltage characterisation was carried out using a probe station (Cascade 11000B) to evaluate the electrical performance of the fabricated LED devices. The EL measurements were performed using a PL mapper (Enlitech) integrated with a two-probe biasing setup, where light was collected through a microscope and coupled to a spectrometer. Temperature-dependent EL measurements were performed using a cryogenic probe station (Janis), equipped with microprobes for bias injection and an optical fiber for light collection, which was coupled to a spectrometer (Andor Technology).

3 Results and discussion

To achieve the design of charge carrier diffusion from indirect bandgap core NWs to direct bandgap branch NWs, we first synthesized core NW arrays with indirect bandgap GaInP by using a TEGa molar fraction of 11.94×10^{-5} during MOVPE growth, as compared to a TEGa molar fraction of 5.97×10^{-5} for direct bandgap core NW growth with the same molar fraction of TMIn as in Tables S1 and S2 in the ESM. According to Ref. [33], $Ga_xIn_{1-x}P$ is a direct bandgap material with x in the range of 0 to 0.68, which corresponds to a bandgap of 1.34 to 1.97 eV, and wavelength from 925 to 624 nm. The XRD data (Fig. S1 in the ESM) from bare core NW array show a Ga composition of x = 83.7%, which indicates indirect bandgap GaInP. Another sample with direct bandgap GaInP NWs with x = 52% Ga in the core was synthesized for the purpose of comparison.

EL measurements under varied bias voltages were performed on both samples to evaluate the emission from core and branches respectively. Both samples are functionally working as charge carrier diffusion induced NW LEDs. The relatively high operating voltage of the LED devices indicates voltage loss through the structure. We previously observed a spatial variation in EL intensity that we attributed to voltage drop in the ITO layer due to its sheet resistance [8].

Room temperature EL spectra for branched NW LEDs having a direct bandgap core exhibit two dominant emission peaks at approximately 645 and 810 nm, as presented in Fig. 2(a). According to the XRD data and previous studies, the 645 nm peak originates from the core NWs, where the GaInP with 52% Ga in the core has a bandgap of 1.92 eV [34], corresponding to 645.8 nm. The other peak at approximately 810 nm is attributed to the emission of branched NWs. At low bias, branch nanowire emission dominates, whereas increasing bias results in a gradual enhancement of the core emission. This arises from the preferential carrier diffusion into the lower bandgap branch NWs, followed by carrier accumulation in the higher bandgap core NWs once the branch states become saturated.

In contrast, branched NW LEDs with indirect bandgap core exhibit markedly different EL characteristics, as shown in Fig. 2(b). At bias lower than 12 V, the EL spectrum of the branched NW LED with indirect bandgap core is dominated by a single emission peak originating from the branch NWs. Because the branch NWs for both the direct and indirect bandgap core NWs were grown under the same molar fractions for all precursors, they ended up

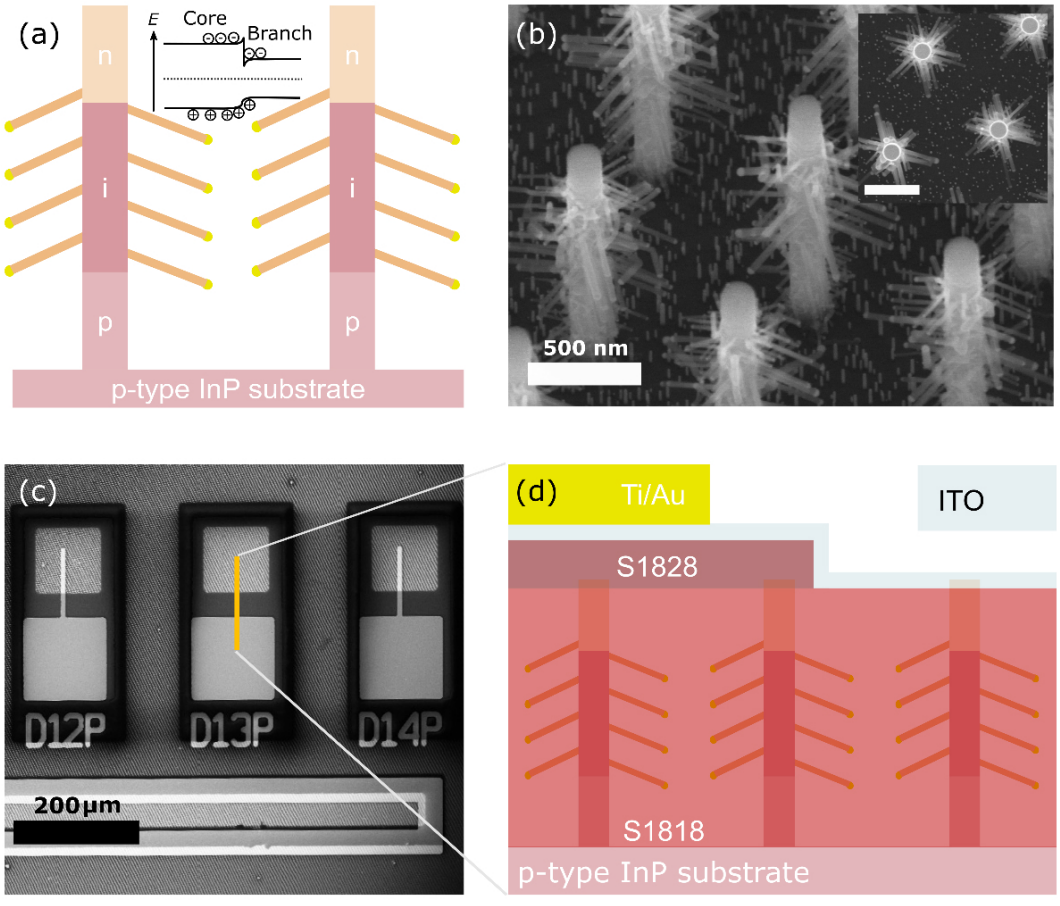

Figure 1 Overview of branched nanowire LEDs: schematic design, morphology, device fabrication, and architecture. (a) Schematic drawing of branched NWs. The inset shows a schematic drawing of the band gap of the heterojunction [31, 32]. (b) SEM image of as-grown branched NWs from a tilted view; the image was obtained at 30° towards the normal of the substrate plane. The inset shows a top-view SEM image with a scale bar of 500 nm. (c) SEM image of three fully processed LED devices with an active area of 100 μm × 100 μm. (d) Schematic drawing of a fully processed device in a cross-sectional view, as indicated by the orange line in (c).

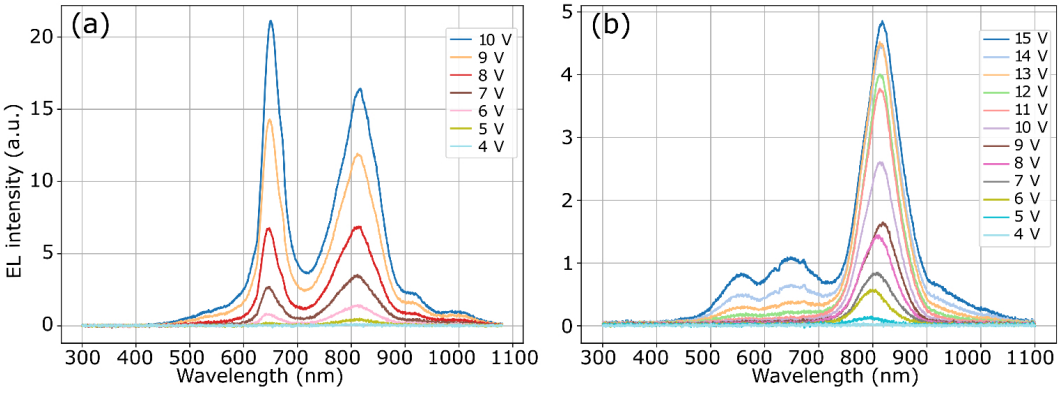

Figure 2 Room temperature EL spectrum of LEDs. (a) EL spectra of branched NW LEDs with direct bandgap core under varied bias. (b) EL spectra of branched NW LEDs with indirect bandgap core under varied bias.

with the same Ga composition, and both emitted at approximately 810 nm. Notably, the branch NW emission is significantly stronger than that of the core NW for the indirect-direct bandgap core-branch architecture. Weak core NW emission was observed at biases above 12 V. With a Ga composition of x = 83.7% in the core $Ga_xIn_{1-x}P$ NWs, it corresponds to an indirect bandgap of 2.24 eV (554 nm) [34], which fits with the first peak from the left, as shown in Fig. 2(b). Another peak appeared at approximately 650 nm, which is approximately 0.33 eV smaller than the peak from the indirect GaInP bandgap. We suspect that this peak originates from donor–acceptor transitions [35, 36].

It is straightforward to compare Figs. 2(a) and 2(b) and determine that the relative intensity of branch emission with respect to core emission is significantly enhanced in branched NW LEDs with an indirect bandgap core as compared to those with a direct bandgap core. The indirect bandgap core NWs have a bandgap of 2.24 eV, while the direct bandgap NWs is about 1.92 eV. Since the branch NWs for both types of LEDs emit around the same wavelength, the bandgap difference between the core and branch NWs in the branched NW LED with indirect bandgap core is larger than with direct bandgap core. Consequently, the diffusion of charge carriers, mainly electrons, will be greater on branched NW LEDs with indirect bandgap core due to a larger band offset, mainly in the conduction band for the used materials system, which leads to the preferred branch NW emission. In indirect bandgap materials, the light absorption is weaker and the charge carrier lifetime is longer [37], which promotes carrier diffusion to the branches and consequently enhances light emission from branch NWs.

One may speculate that the branch NW emissions can arise from the absorption of the light emitted from the core NWs to be re-emitted in the branch NWs instead of being a result of charge carrier diffusion from the core to the branch where recombination will give rise to EL. The absence of the core NW peak but with a strong emission peak from branch NWs demonstrates that the luminescence from these NW LEDs is induced by charge carrier diffusion instead of secondary branch emissions. Devices with direct bandgap cores exhibit higher total integrated emission intensity compared to those with indirect bandgap cores. However, it should be noted that indirect bandgap materials are intrinsically more resistive, resulting in higher operating bias voltages and lower injection currents through these NWs, as shown in Fig. S2 in the ESM. Consequently, the absolute emission counts from branch NW LEDs with indirect bandgap core appear lower.

To investigate the mechanism of carrier recombination and light emission from indirect to direct bandgap material in more detail, temperature-dependent EL measurements were performed, as displayed in Fig. 3. A constant current of 20 mA was applied for characterization of the NW LEDs with direct bandgap cores to avoid the temperature-dependent contact resistance. This current was too high for the indirect bandgap cores due to the higher NW resistivity, and limits of the source measure unit (SMU, Keithly 2636B), which is why we opted for the use of a constant voltage. It can be observed that the intensity of both the direct bandgap core NWs and the branch NWs peak decrease with increased temperatures, as shown in Fig. 3(a). While in Fig. 3(b) only the branch NWs peak shows the same trend and the other peaks coming from the indirect bandgap core NWs showed the opposite

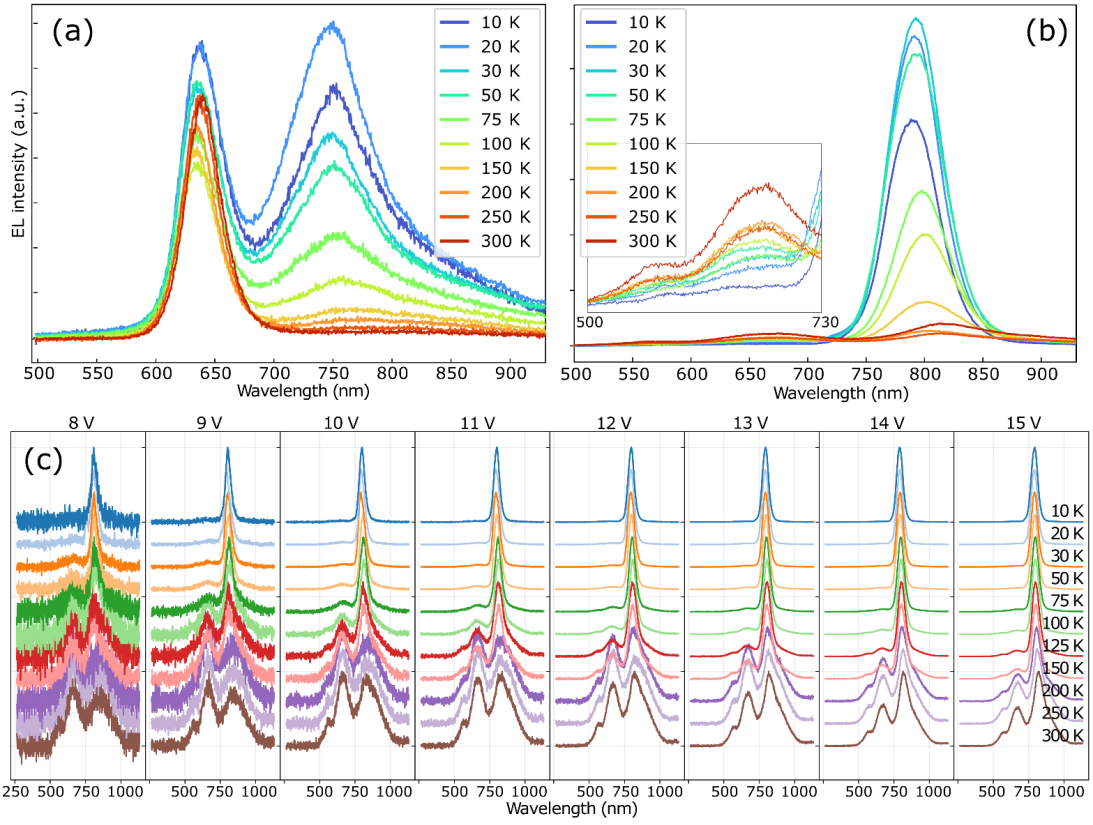

Figure 3 Temperature-dependent EL spectra of LEDs. (a) Branched NW LED with direct bandgap core under applied current of 20 mA, and (b) branched NW LED with indirect bandgap core under applied bias of 14 V. The inset is a zoomed in picture of this EL spectra in wavelength range of 500 to 730 nm. (c) Normalized temperature-dependent EL spectra of branched NW LEDs with indirect bandgap under varied bias.

as depicted in the inset. Direct bandgap materials, as in both the core and the branch NWs in Fig. 3(a) and the branch NWs in Fig. 3(b) generally show strong direct bandgap recombination at low temperatures. At higher temperatures, the peak redshifts owing to shrinkage of bandgaps and its intensity decreases owing to increased Shockley-Read-Hall (SRH) recombination via the nanowire free surface at higher temperatures [38]. Surface defects can freeze out at lower temperatures, enhancing radiative recombination at low temperatures but act as nonradiative recombination centers in semiconductor materials, resulting in low device efficiency. Since the surface recombination centers are thermally activated, the contribution of surface defect mediated recombination is strongly suppressed at low temperature [39]. Thus, the peak intensity decreases as the temperature increases. However, as the peaks at approximately 554 and 650 nm are resulting from the indirect bandgap core NWs, both peaks are thermally activated [40]. Therefore, their intensity increased with increasing temperature owing to an increase in the phonon population. In the low-temperature regime (10–30 K), a slight increase in emission intensity from the branch NWs is observed for both direct and indirect bandgap core NW LEDs. This behavior is attributed to more efficient carrier injection upon heating, resulting from reduced carrier localization and decreased electrical contact resistance with increasing temperatures.

Figure 3(c) shows the normalized temperature-dependent EL spectra of the branched NW LED with indirect bandgap core measured from 10 to 300 K under bias from 8 to 15 V. The peaks at longer wavelength originating from the branch NWs show up at all temperatures and applied voltages. However, the peak at the shortest wavelength originating from the core NWs was only visible at temperatures higher than 75 K. It seems that the core peak is slightly stronger than the branch peak at room temperature for bias voltages below 9 V, which we attribute to inefficient current injection resulting in less carrier diffusion into branches. The branch emission dominates once the bias voltage is increased beyond 9 V.

The relationship between the EL peak energy and the linewidth from the branch NWs to the temperature is displayed in Figs. 4(a) and 4(b). The EL peak red shifts as the temperature is increased. The red shift with increasing temperatures originates from the shrinkage of bandgap as described by Varshni relation [38]. At constant temperature, increasing the applied voltage and injection current leads to a slight blueshift of the emission peak, which is attributed to band filling in the branch nanowires. The plot of relationship between the peak energy of the branch NWs to the current density is displayed in Fig. S3 in the ESM, where a peak shift less than 40 meV was observed with 2 orders difference in current density. The emission linewidth, characterized by the full width at half maximum (FWHM), increases with temperature due to thermal broadening.

Current–voltage (I–V) characteristics have been carried out on multiple devices on the same sample for branched NW LEDs with direct and indirect bandgap core. Figure 5(a) displays the I–V curve of one 100 μm × 100 μm LED, with a semilogarithmic plot in the inset where data were fitted by use of the ideal diode equation to extract the ideality factor and dark saturation current. Both the LEDs with direct and indirect bandgap core exhibit rectifying behavior, confirming the functional pin junction in the array of core NWs. As compared to the I–V curve for the LED with direct bandgap core, the LED with indirect bandgap core NWs presents a premature turn-on, while the LED with direct bandgap core NWs has a more abrupt onset. This is attributed to shunt leakage paths arising from surface-related defects that exist in parallel with the p-n junction. Such leakage paths account for the current in the indirect bandgap core device to be higher than in the direct bandgap core device at bias voltages below 5 V. At higher bias voltages, the effect of series resistance becomes dominant, leading to a reduced current through the indirect bandgap NWs as compared to the direct bandgap one, as discussed previously.

After fitting by using the voltage range between 0.3 to 0.6 V in the linear part of the semi logarithmic I–V curve, as highlighted red and green color in the inset of Fig. 5(a) to the ideal diode equation, the distribution of ideality factor and saturation current is plotted and shown in Fig. 5(b). The wide distribution of ideality factors originates from local defects during synthesis and fabrication of the devices, most probably due to inhomogeneities in core NW synthesis. For LEDs on the sample with direct bandgap core, most of the ideality factors distribute between 3 to 4, while they were evaluated to be in-between 4 to 6 for LEDs with indirect bandgap core. The higher Ga composition in the indirect bandgap core NWs leads to more deep traps and increased nonradiative recombination [41], which results in higher ideality factors. The higher ideality factor can originate from higher series resistance as well, due to difficulties making electrically transparent contacts to the indirect bandgap material. The increased dark saturation current in LEDs with indirect bandgap cores provides additional evidence for shunt leakage paths, in agreement with the earlier turn-on behavior and elevated current at low bias voltages. It should be noted that

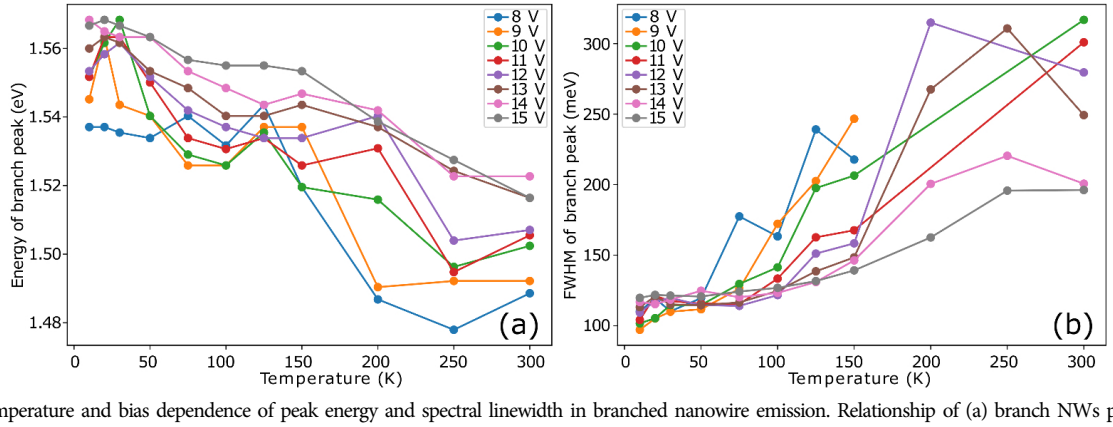

Figure 4 Temperature and bias dependence of peak energy and spectral linewidth in branched nanowire emission. Relationship of (a) branch NWs peak energy to temperature under varied bias and (b) branch NWs peak linewidth to temperature under varied bias.

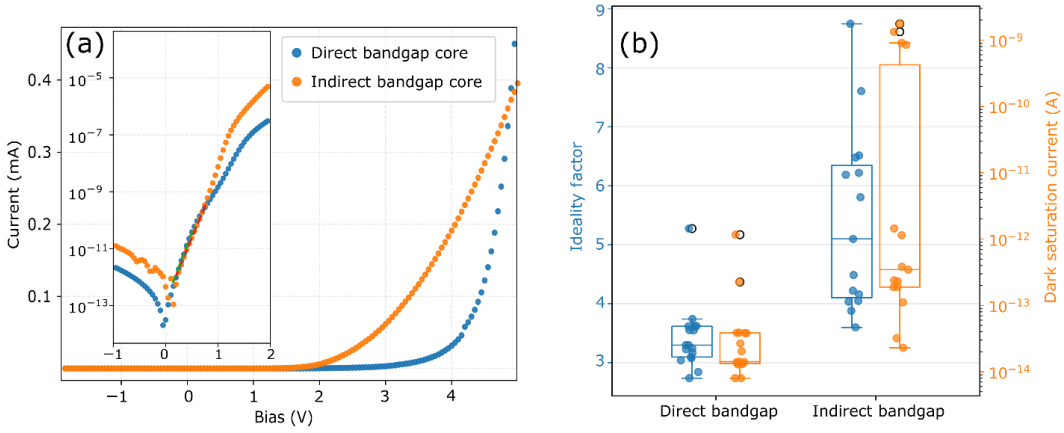

Figure 5 Electrical characteristics of branched nanowire LEDs with direct and indirect bandgap cores. (a) Current–voltage characteristic of branched NW LEDs with direct and indirect bandgap core NWs. Inset is the data plotted using a semi logarithmic scale. (b) Distributions of fitted ideality factor and dark saturation current.

challenges remain in forming high-quality electrical contacts to the GaInP NW tips [27], especially for nanowires with a relatively high and indirect bandgap that results in non-ideal LED performance. The observed electrical characteristics highlight the need for improved contact engineering and more effective surface passivation strategies.

Relative external quantum efficiency (EQE) is calculated by normalizing the value of integrated EL intensity over current density at different temperatures and biases to the maximum value, as shown in Fig. 6. Here, the current density is calculated depending on the total area of the footprints of core NW arrays. Conventional planar nitride-based LEDs are often affected by efficiency droop with increasing current density, owing to significant Auger recombination and current overflow [42]. However, this effect was not observed on our branched NW LEDs. At this point, we cannot rule out that nonradiative surface recombination is the dominating loss process.

4 Conclusions

In conclusion, we have demonstrated charge carrier diffusion induced NW LEDs using indirect bandgap GaInP core NWs and with direct bandgap GaInP branch NWs. EL predominantly originating from the branch NWs was observed. Owing to the larger bandgap difference between the core and branch NWs, as well as the longer carrier lifetime in indirect bandgap materials, the charge carrier diffusion is enhanced. Therefore, a strongly enhanced branch emission and effective suppression of core emission were achieved using an indirect core NW in the LEDs. Temperature-dependent EL measurements reveal fundamentally different recombination behaviors in the direct and indirect bandgap core NWs. The EL intensity decreases for direct bandgap core and branch NWs with increasing temperatures, while it increases for indirect bandgap NWs due to increased population of thermally activated phonon. The branch emission exhibits a modest red shift and linewidth broadening with temperature increasing, which indicates a good spectral stability. Moreover, the branched NW LEDs show increasing EQE with current density. While *I*–*V* characteristics suggest that further improvements in surface passivation and contact optimization are needed, this work opens the possibility of building branched NW LEDs for quasi-monochromatic light emission with tunable wavelength and establishes charge carrier diffusion induced NW LEDs as an attractive candidate for high efficiency light emitters.

Electronic Supplementary Material: Supplementary material (precursor molar fractions used for nanowire synthesis, corresponding XRD characterization, electrical characterization, and analysis of branch emission peak energy) is available in the online version of this article at https://doi.org/10.26599/NR.2026.94908799.

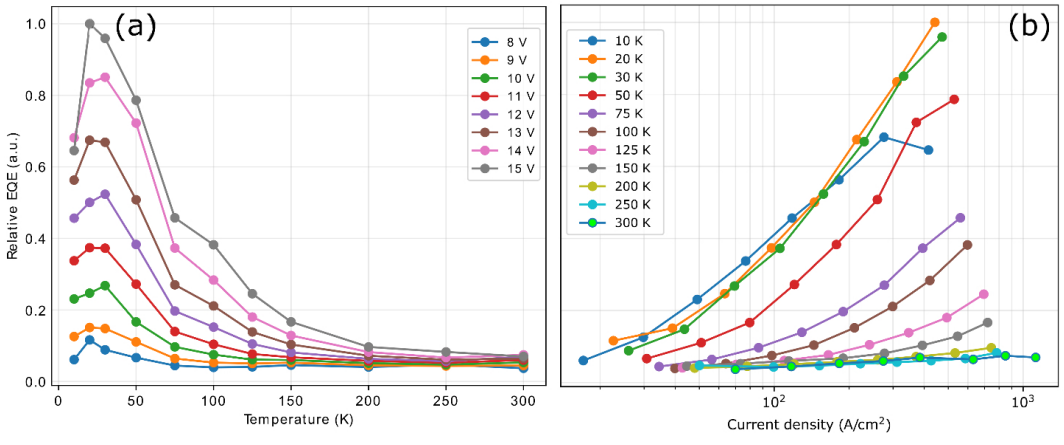

Figure 6 Relative EQE and the relationship between (a) temperature and (b) current density.

Data availability

All data needed to support the conclusions in the paper are presented in the manuscript and the Electronic Supplementary Material. Additional data related to this paper may be requested from the corresponding author upon request.

Acknowledgements

This work was performed within NanoLund at Lund University. It was supported by Myfab. This work has received funding from the Swedish Research Council, the Swedish Energy Agency, the European Union's Horizon 2020 Research and Innovation Program under the Marie Skłodowska-Curie grant agreement No. 945378, the Wallenberg Initiative Materials Science for Sustainability (WISE) funded by the Knut and Alice Wallenberg Foundation and the Royal Physiographic Society in Lund. We thank Associate Professor Claes Thelander for assistance with the cryogenic probe station setup.

Declaration of competing interest

All the contributing authors report no conflict of interests in this work.

Author contribution statement

Y. Z.: Data curation, writing – original draft, validation, experimental design. K. A.: Validation, experimental design, writing – review & editing. H. N. C.: Validation, data curation, writing – review & editing. M. T. B.: Project administration, funding acquisition, supervision, writing – review & editing. All the authors have approved the final manuscript.

Use of AI statement

None.

References

[1] Wallentin, J.; Anttu, N.; Asoli, D.; Huffman, M.; Åberg, I.; Magnusson, M. H.; Siefer, G.; Fuss-Kailuweit, P.; Dimroth, F.; Witzigmann, B. et al. InP nanowire array solar cells achieving 13.8% efficiency by exceeding the ray optics limit. *Science* **2013**, *339*, 1057–1060.

[2] Cui, Y. C.; Wang, J.; Plissard, S. R.; Cavalli, A.; Vu, T. T. T.; van Veldhoven, R. P. J.; Gao, L.; Trainor, M.; Verheijen, M. A.; Haverkort, J. E. M. et al. Efficiency enhancement of InP nanowire solar cells by surface cleaning. *Nano Lett.* **2013**, *13*, 4113–4117.

[3] Yao, M. Q.; Huang, N. F.; Cong, S.; Chi, C. Y.; Seyedi, M. A.; Lin, Y. T.; Cao, Y.; Povinelli, M. L.; Dapkus, P. D.; Zhou, C. W. GaAs nanowire array solar cells with axial p-i-n junctions. *Nano Lett.* **2014**, *14*, 3293–3303.

[4] Karimi, M.; Jain, V.; Heurlin, M.; Nowzari, A.; Hussain, L.; Lindgren, D.; Stehr, J. E.; Buyanova, I. A.; Gustafsson, A.; Samuelson, L. et al. Room-temperature InP/InAsP quantum discs-in-nanowire infrared photodetectors. *Nano Lett.* **2017**, *17*, 3356–3362.

[5] Ren, D. K.; Meng, X.; Rong, Z. X.; Cao, M.; Farrell, A. C.; Somasundaram, S.; Azizur-Rahman, K. M.; Williams, B. S.; Huffaker, D. L. Uncooled photodetector at short-wavelength infrared using InAs nanowire photoabsorbers on InP with p-n heterojunctions. *Nano Lett.* **2018**, *18*, 7901–7908.

[6] Yang, I.; Kim, S.; Niihori, M.; Alabadla, A.; Li, Z. Y.; Li, L.; Lockrey, M. N.; Choi, D. Y.; Aharonovich, I.; Wong-Leung, J. et al. Highly uniform InGaAs/InP quantum well nanowire array-based light emitting diodes. *Nano Energy* **2020**, *71*, 104576.

[7] Ra, Y. H.; Lee, C. R. Core–shell tunnel junction nanowire white-light-emitting diode. *Nano Lett.* **2020**, *20*, 4162–4168.

[8] Zhao, Y.; Adham, K.; Hessman, D.; Borgström, M. T. Direct band gap white light emission from charge carrier diffusion induced nanowire light-emitting diodes. *Nano Energy* **2024**, *132*, 110400.

[9] Saxena, D.; Mokkapati, S.; Parkinson, P.; Jiang, N.; Gao, Q.; Tan, H. H.; Jagadish, C. Optically pumped room-temperature GaAs nanowire lasers. *Nat. Photonics* **2013**, *7*, 963–968.

[10] Azimi, Z.; Gagrani, N.; Qu, J. T.; Lem, O. L. C.; Mokkapati, S.; Cairney, J. M.; Zheng, R. K.; Tan, H. H.; Jagadish, C.; Wong-Leung, J. Understanding the role of facets and twin defects in the optical performance of GaAs nanowires for laser applications. *Nanoscale Horiz.* **2021**, *6*, 559–567.

[11] Björk, M. T.; Ohlsson, B. J.; Sass, T.; Persson, A. I.; Thelander, C.; Magnusson, M. H.; Deppert, K.; Wallenberg, L. R.; Samuelson, L. One-dimensional steeplechase for electrons realized. *Nano Lett.* **2002**, *2*, 87–89.

[12] Gudiksen, M. S.; Lauhon, L. J.; Wang, J. F.; Smith, D. C.; Lieber, C. M. Growth of nanowire superlattice structures for nanoscale photonics and electronics. *Nature* **2002**, *415*, 617–620.

[13] Yan, R. X.; Gargas, D.; Yang, P. D. Nanowire photonics. *Nat. Photonics* **2009**, *3*, 569–576.

[14] Akamatsu, T.; Tomioka, K.; Motohisa, J. Demonstration of InP/InAsP/InP axial heterostructure nanowire array vertical LEDs. *Nanotechnology* **2020**, *31*, 394003.

[15] Anand, N.; Ghosh, D. K.; Abbes, A.; Kundu, M.; Rahman, M. A.; Jenson, C. G.; Morandotti, R.; Baten, M. Z.; Sadaf, S. M. Ultra-dense green InGaN/GaN nanoscale pixels with high luminescence stability and uniformity for near-eye displays. *ACS Nano* **2024**, *18*, 26882–26890.

[16] Kivisaari, P.; Berg, A.; Karimi, M.; Storm, K.; Limpert, S.; Oksanen, J.; Samuelson, L.; Pettersson, H.; Borgström, M. T. Optimization of current injection in AlGaInP core-shell nanowire light-emitting diodes. *Nano Lett.* **2017**, *17*, 3599–3606.

[17] Anttu, N.; Xu, H. Q. Coupling of light into nanowire arrays and subsequent absorption. *J. Nanosci. Nanotechnol.* **2010**, *10*, 7183–7187.

[18] Monemar, B.; Ohlsson, B. J.; Gardner, N. F.; Samuelson, L. Chapter seven-nanowire-based visible light emitters, present status and outlook. *Semicond. Semimetals* **2016**, *94*, 227–271.

[19] Barrigón, E.; Heurlin, M.; Bi, Z. X.; Monemar, B.; Samuelson, L. Synthesis and applications of III-V nanowires. *Chem. Rev.* **2019**, *119*, 9170–9220.

[20] Behrman, K.; Kymissis, I. Micro light-emitting diodes. *Nat. Electron.* **2022**, *5*, 564–573.

[21] Kivisaari, P.; Chen, Y.; Anttu, N. Emission enhancement, light extraction and carrier dynamics in InGaAs/GaAs nanowire arrays. *Nano Futures* **2018**, *2*, 015001.

[22] Anttu, N. Modifying the emission of light from a semiconductor nanowire array. *J. Appl. Phys.* **2016**, *120*, 043108.

[23] Adham, K.; Zhao, Y.; Kivisaari, P.; Borgström, M. T. Characterization of N-doped branches in nanotree LEDs. *Energy Adv.* **2024**, *3*, 2922–2928.

[24] Sze, S. M.; Ng, K. K. *Physics of Semiconductor Devices*; 3rd ed. Wiley-Interscience: Hoboken, 2007.

[25] Hrachowina, L.; Anttu, N.; Borgström, M. T. Wafer-scale synthesis and optical characterization of InP nanowire arrays for solar cells. *Nano Lett.* **2021**, *21*, 7347–7353.

[26] Otnes, G.; Heurlin, M.; Graczyk, M.; Wallentin, J.; Jacobsson, D.; Berg, A.; Maximov, I.; Borgström, M. T. Strategies to obtain pattern fidelity in nanowire growth from large-area surfaces patterned using nanoimprint lithography. *Nano Res.* **2016**, *9*, 2852–2861.

[27] Wallentin, J.; Barrutia Poncela, L.; Jansson, A. M.; Mergenthaler, K.; Ek, M.; Jacobsson, D.; Reine Wallenberg, L.; Deppert, K.; Samuelson, L.; Hessman, D. et al. Single GaInP nanowire p-i-n junctions near the direct to indirect bandgap crossover point. *Appl. Phys. Lett.* **2012**, *100*, 251103.

[28] Berg, A.; Lenrick, F.; Vainorius, N.; Beech, J. P.; Wallenberg, L. R.; Borgström, M. T. Growth parameter design for homogeneous material composition in ternary $Ga_xIn_{1-x}P$ nanowires. *Nanotechnology* **2015**, *26*, 435601.

[29] Adham, K.; Zhao, Y.; Hrachowina, L.; Alcer, D.; Wallenberg, R.; Borgström, M. T. Growth of branched nanowires via solution-based Au seed particle deposition. *Mater. Res. Express* **2023**, *10*, 085003.

[30] Zhang, Y. W.; Chen, Y.; Hrachowina, L.; Sundvall, C.; Åberg, I.; Borgström, M. UV exposure: A novel processing method to fabricate nanowire solar cells. In *2019 IEEE 46th Photovoltaic Specialists Conference (PVSC)*, Chicago, IL, USA, 2019, pp 2646–2648.

[31] Piprek, J. Electron energy bands. In *Semiconductor Optoelectronic Devices*. Piprek, J., Ed.; Elsevier: Amsterdam, 2003; pp 13–48.

[32] Tiwari, S.; Frank, D. J. Empirical fit to band discontinuities and barrier heights in III-V alloy systems. *Appl. Phys. Lett.* **1992**, *60*, 630–632.

[33] Merle, P.; Auvergne, D.; Mathieu, H.; Chevallier, J. Conduction band structure of GaInP. *Phys. Rev. B* **1977**, *15*, 2032–2047.

[34] Adachi, S. *Properties of Semiconductor Alloys: Group-IV, III-V and II-VI Semiconductors*; John Wiley & Sons, Ltd: Chichester, 2009.

[35] Grimmeiss, H. G.; Rabenau, A.; Koelmans, H. Some properties of p-n junctions in GaP. *J. Appl. Phys.* **1961**, *32*, 2123–2127.

[36] Dierschke, E. G.; Pearson, G. L. Effect of the donor concentration on the green electroluminescence from gallium phosphide diodes. *J. Appl. Phys.* **1970**, *41*, 321–328.

[37] Pankove, J. I. *Optical Processes in Semiconductors*; Dover: New York, 1975.

[38] Varshni, Y. P. Temperature dependence of the energy gap in semiconductors. *Physica* **1967**, *34*, 149–154.

[39] Imangholi, B.; Hasselbeck, M. P.; Sheik-Bahae, M.; Epstein, R. I.; Kurtz, S. Effects of epitaxial lift-off on interface recombination and laser cooling in GaInP/GaAs heterostructures. *Appl. Phys. Lett.* **2005**, *86*, 081104.

[40] Wang, C.; Wang, B.; Made, R. I.; Yoon, S. F.; Michel, J. Direct bandgap photoluminescence from N-type indirect GaInP alloys. *Photonics Res.* **2017**, *5*, 239–244.

[41] Zhang, W.; Zeng, X. L.; Su, X. J.; Zou, X. S.; Mante, P. A.; Borgström, M. T.; Yartsev, A. Carrier recombination processes in gallium indium phosphide nanowires. *Nano Lett.* **2017**, *17*, 4248–4254.

[42] Schubert, E. F. *Light-Emitting Diodes*; 4th ed. Cambridge University Press: Cambridge, 2018.